Crystallography, magnetism, and band structure of $Mn_5Ni_2Bi_4$-type compounds*

J. C. Suits, G. B. Street, and Kenneth Lee
IBM Research Laboratory, San Jose, California 95193

J. B. Goodenough
Lincoln Laboratory, Massachusetts Institute of Technology, Lexington, Massachusetts 02.73

(Received 7 February 1974)

The crystal structure, magnetic properties, and a schematic band structure have been determined for the new class of magnetic compounds of the type $Mn_5Ni_2Bi_4$. This class includes $Mn_5Pd_2Bi_4$, $Mn_5Rh_2Bi_4$, and $Mn_3Cu_4Bi_4$. The structure has been calculated with the aid of Patterson and difference Patterson analysis of powder x-ray diffraction data. The spontaneous magnetic moment at 4.2 K for these compounds lies in the range 50–64 emu/g and Curie temperatures range between -7 °C and 183 °C. Molar Curie constants have been measured. A schematic band-structure model has been determined. It is based on local-site symmetries and includes both strongly correlated and itinerant d electrons. As in the Heusler and Ni_3Mn alloys, antiferromagnetic coupling of a small percentage of Mn-atom moments appears to be associated with atomic disorder. Within the experimental limits of apparent atomic ordering, the magnetization and Curie constants predicted from the band model are in agreement with experiment.

I. INTRODUCTION

A new class of magnetic compounds has recently been reported.[1] The chemical formulas are $Mn_5X_2Bi_4$ for X = Ni, Pd, or Rh, and $Mn_3Cu_4Bi_4$. X-ray diffraction spectra indicate that all four compounds have essentially the same structure. This crystal structure had not been previously reported. These compounds show large spontaneous magnetization with Curie temperatures ranging between −7 °C and 183 °C.

This paper presents an interpretation of the magnetic properties of these compounds. This interpretation is based on a schematic density-of-states–versus–energy diagram derived according to principles described previously.[2,3] Since this derivation requires a precise knowledge of the crystal structure, we first describe the structure and the evidence used in the structure determination. We next review the experimental measurements of low-temperature moment and high-temperature susceptibility. The schematic density-of-states curve is then derived. Finally, quantitative predictions that follow from this qualitative analysis are compared with the magnetic data.

II. CRYSTALLOGRAPHY

Single crystals of these materials were not available, and hence it was necessary to determine the crystal structures entirely from powder data. It is well known that it is in general very difficult to obtain precision structure data from powder patterns because of the overlapping reflections; however, the Patterson projections yielded useful information for this structure.

The experimental methods used were as follows: A Norelco vertical-plane scanning diffractometer[4] (modified to include a long parallel slit collimator), a vacuum path and specimen chamber,[5] and a diffracted beam focusing graphite monochromator were used. The specimen was rotated continuously in its own plane to reduce crystallite statistical errors. A copper tube operated at 50 kV and 25 mA was used with an angular aperture of 4° in the back-reflection region and 1° in the front-reflection region. A portion of the pattern was recorded with both apertures to obtain the scaling factor. The diffractometer was controlled by an IBM System 7 computer and the pattern was scanned using 0.05° (2θ) steps and a 2-sec counting time per step. The data were recorded on disk and transferred to an IBM 360/195 computer for analysis. A curve-fitting method was used to provide peak positions, based on all data points in each line profile, and integrated intensities.[6] These experimental integrated intensities were measured and provided by Taupin and Parrish. The pattern was indexed using Taupin's method.[7]

The diffractometer patterns of $Mn_5Ni_2Bi_4$ and $Mn_5Pd_2Bi_4$ are shown in Figs. 1(a) and 1(c). They are both cubic with a lattice parameter ≈ 12 Å. This cubic cell contains eight $Mn_5X_2Bi_4$ units.

A (001) Patterson projection was calculated first by assuming that all ambiguous lines [overlapping ($hk0$) and (hkl)] were entirely due to ($hk0$) [Fig. 2(a)] and second by assuming that all ambiguous lines have no ($hk0$) contribution. The general features of the two projections were similar, differing only in peak shape and peak height. These projections suggest a two-sublattice structure. One sublattice has a large electron density and the other a much smaller electron density. Since the Bi atom has a much higher atomic number than any of the other atoms and since the Patterson function is proportional to the square of electron density, it is

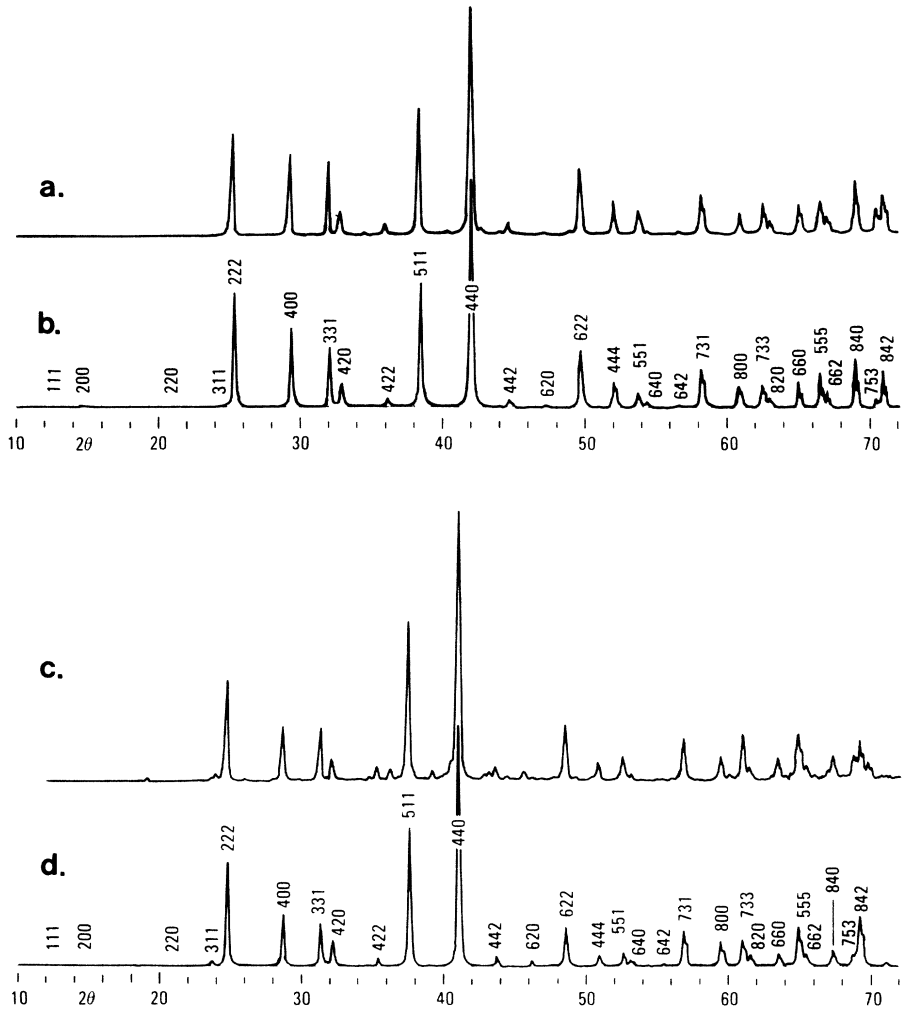

FIG. 1. X-ray diffractometer data, intensity vs 2θ (deg), for $Mn_5Ni_2Bi_4$ [(a) experimental, (b) calculated] and $Mn_5Pd_2Bi_4$ [(c) experimental, (d) calculated]. CuKα radiation. The vertical sensitivity was increased by a factor of 2 at 31° and again another 2 at 65° for all curves in order to facilitate comparison of higher angle lines

likely that Bi occupies the first sublattice.

Next, a difference Patterson[8] was calculated using the X=Ni and X=Pd diffractometer data. The result, shown in Fig. 2(b), is again a projection onto the (001) plane. It essentially shows the projected vectors from the replaceable atom, which is set at the origin, to the other atoms in the crystal. The pronounced atom positions in Fig. 2(b) therefore represent the heavy Bi atoms relative to the Ni or Pd atom positions. This suggests that the Ni or Pd atoms are on the $\frac{1}{8}$, $\frac{1}{8}$ positions in Fig. 2(a). Some caution must be exercised because we are dealing with polycrystals and because Patterson maps do not give electron density directly.

From the systematic absences in the reflections given in Fig. 1, the unit cell was found to be face-centered cubic with the following space groups possible: $F23$, $Fm3$, $F432$, $F4_132$, $F\bar{4}3m$, and $Fm3m$. Since $F432$ differs from $Fm3m$ only in point groups containing 96 or more atoms, we need not consider $F432$ further.

Except for 48-fold groups or higher, which we also ignore, all point groups may be described in terms of the point groups $4a$-$24g$ of space group $F\bar{4}3m$. To describe in this notation the sublattices observed in Fig. 2, we use $x \approx \frac{1}{4}$ for $24f$, $x \approx 0$ for $24g$, and $x \approx \frac{1}{8}$, $\frac{3}{8}$, $\frac{5}{8}$, $\frac{7}{8}$ for $16e$. We will call them

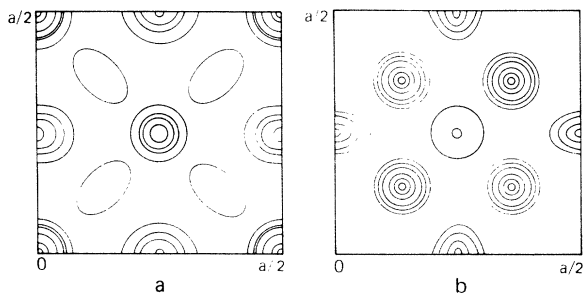

FIG. 2. (a) (001) Patterson projection for powder sample of $Mn_5Ni_2Bi_4$. (b) Difference Patterson using $Mn_5Ni_2Bi_4$ and $Mn_5Pd_2Bi_4$. All overlapping lines are assumed to contribute fully to ($hk0$).

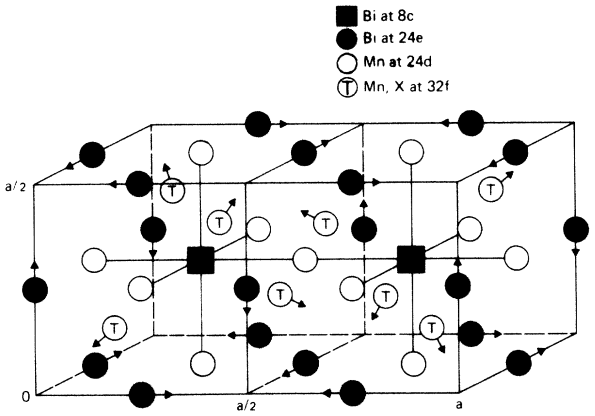

FIG. 3. Structure of $Mn_5Ni_2Bi_4$. Two octants of the unit cell are shown. The other octants have one or the other of these two structures and are arranged so that no two adjacent octants have the same atomic arrangement.

f, g, e_1, e_2, e_3, and e_4, respectively, and the approximation sign is to allow distortions of the sublattice atoms about these "ideal" lattice positions. As suggested by the Patterson analysis, the 32 Bi will be placed on one sublattice. In terms of the above notation, this means all Bi are on either $24f+4c+4d$ or $16e_1+16e_3$ (or permutations).

Symmetry factors[9] have been calculated for the $4a$-$24g$ point groups in $F\bar{4}3m$ for small distortions about the two-sublattice model. The remainder of the analysis consists of calculating structure factors using these symmetry factors for the zero-intensity (111), (200), and (220) lines, for the (331) line, which is absent for X=Ni, and for various other nonzero lines of importance. This is essentially a trial and error procedure, but a number of simplifications are possible. (i) Consideration of the symmetry factors for the (111) and (331) lines shows that they are identical except for distortion. Since (111) has zero intensity and (331) is a strong line, this means that it is essential to include distortion in this structure. (ii) Consideration of the (200) and (420) lines in a similar manner indicates that Bi-atom displacements are more likely along ⟨100⟩ than along ⟨111⟩. This suggests that Bi is on $24f+4c+4d$. (iii) The difference Patterson has indicated that 16 Ni or 16 Pd are on the other sublattice from the Bi and therefore on e sites; the final location is $\frac{1}{2}(e_1+e_4)$. The Mn are found to fill the remaining $\frac{1}{2}(e_1+e_4)$ sites and also the $24g$ sites. The $4a$ and $4b$ sites remain empty.

Comparison of these site occupations with the other allowed space groups shows that the highest-allowed symmetry group is $Fm3m$. In terms of $Fm3m$ notation, the final structure is Bi – $8c$, Bi – $24e$ (x = 0.285 for X=Ni and 0.290 for X=Pd), Mn – $24d$, and (16Mn+16X) – $32f$ (x = 0.104 for X =Ni and 0.114 for X=Pd). The final structure is shown in Fig. 3. This structure is remarkably well indicated by the projections shown in Fig. 2.

In this structure the 32 Bi atoms in the unit cell form a fcc sublattice with a sublattice constant equal to one-half the lattice constant of the unit cell. The remaining sites may be described as octahedral or tetrahedral relative to the Bi sublattice. There are 32 octahedral sites; 24 of these ($24d$) are filled by Mn. Of the 64 tetrahedral sites, 32 are filled ($32f$ with 16 Mn and 16X, X=Ni or Pd). There is considerable distortion about the empty octahedral sites as indicated by the arrows in Fig. 3.

The chemical composition of the Cu compound is different than that of Ni or Pd, so the difference Patterson analysis cannot be applied. Also, since the scattering factors of Mn and Cu are very similar, it has not been possible to determine experimentally the location of the copper. However, a reasonable assignment, by comparison with the Ni and Pd compounds, is Cu on the tetrahedral sites. The X=Rh compound has not been prepared in single-phase quality, so no structure work has been done on it.

Theoretical diffraction patterns calculated by the Smith program,[10] based on the model of Fig. 3, are shown in Fig. 1. (A table of calculated and observed integrated intensities has been published.)[1] The apparent good agreement between the experimental and calculated patterns is confirmed by the residual factor ($\sum|I_0-I_c|/\sum I_0$) based on these intensities. From the first 52 lines, a residual factor of 0.16 was calculated for both X=Ni and X =Pd with no temperature or other corrections included.

III. MAGNETIC PROPERTIES

The magnetic properties of these compounds were measured using a PAR vibrating-sample magnetometer. This magnetometer was modified by mounting a thermocouple directly on the vibrating sample rod with the thermocouple junction essentially in contact with the sample to ensure accurate sample-temperature measurements. Also, provision was made to allow measurements with the sample chamber evacuated.

A magnetization-versus-field loop taken using $Mn_5Ni_2Bi_4$ at room temperature is shown in Fig. 4. The coercive force of all four of these compounds is in the range 100–200 Oe. Measurements at 4.2 K are shown in Fig. 5. It is interesting to note that the Ni compound shows a much steeper approach to saturation at 4.2 K than at 68 K. It seems likely that some antiparallel spin alignment is occurring in this compound below 68 K. It will be seen later that comparison of low-temperature

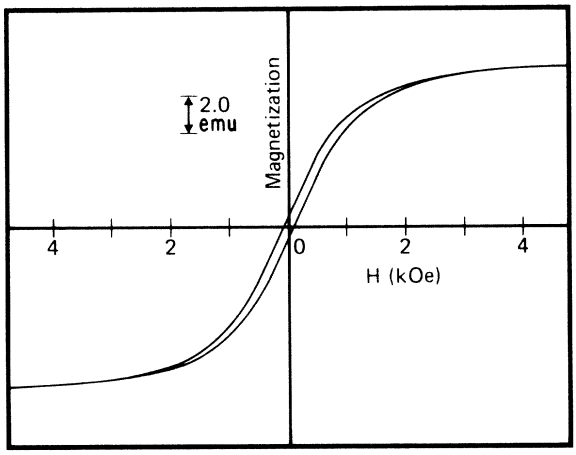

FIG. 4. Magnetization vs applied field for powder sample of $Mn_5Ni_2Bi_4$ at room temperature. The sample weight is 291 mg.

moment with high-temperature susceptibility suggests there may be a small fraction of antiparallel spins at low temperature for all four compounds. The saturation magnetization at 4.2 K is shown in Table I and is derived from these curves by plotting magnetization as a function of H^{-1} and extrapolating to the intercept at $H^{-1}=0$. We have also plotted magnetization as a function of H^{-2} (approach to saturation primarily due to anisotropy) in addition to H^{-1} (approach to saturation primarily due to imperfections)[11] and have found that over the available range of field it is not possible to distinguish between these two methods. Both methods give the same saturation magnetization to within 1%.

Reciprocal susceptibility versus temperature is shown in Fig. 6. The curve for $X=$Cu shows a transition at 280 °C from one straight line to a second line nearly parallel to the first. Depending upon sample heat treatment, data along either of the two lines alone have been obtained over this entire temperature interval. This effect may be due to temperature-dependent ordering of the Mn and Cu between the octahedral and tetrahedral sites.

TABLE I. Magnetic properties of Mn-X-Bi compounds.

X	a(Å)	θ(°C)	T_c(°C)	σ^a(emu/g)	σ_s(emu/g)	C_{mole}
Ni	12.16	108	101	39.4	64	12.4
Cu	12.18	202	183	39.3	50.5	8.3($T>280$ °C) 8.7($T<280$ °C)
Rh	12.31	···	−7	···	···	···
Pd	12.44	67	54	28.0	58	12.7

[a] 20 ° C, 20 kOe.

IV. INTERPRETATION OF MAGNETIC PROPERTIES

Interpretation of the magnetic properties of these compounds requires a knowledge of the number n_d of outer d electrons per formula unit, the relative stabilities of the various d bands, and the ability to distinguish strongly correlated from itinerant d electrons.

Each atom has one outer s and three outer p orbitals, each orbital having a twofold-spin degeneracy. Interaction between the metal and metalloid sublattices creates bonding and antibonding states as well as states that are nonbonding with respect to the metal-metalloid interactions. The formula units $Mn_2X_2[Mn_3]Bi_4$ and $Cu_4[Mn_3]Bi_4$ contain 32 6s and 6p states at Bi atoms and 56 s and p states at the metal atoms. Therefore, there are 32 bonding, 32 antibonding, and 24 nonbonding s and p states. Because the metalloid Bi atoms are electronegative

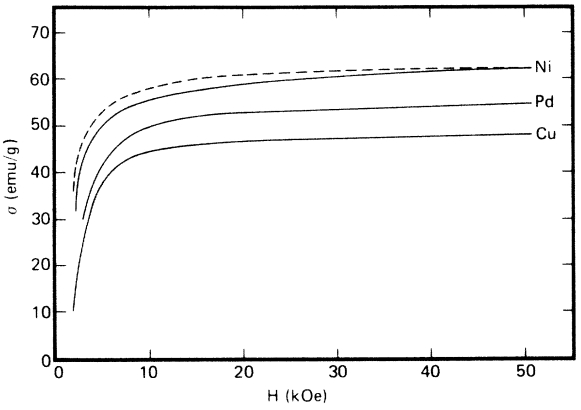

FIG. 5. Magnetization vs applied field for the Ni, Pd, and Cu compounds at 4.2 K. The dashed curve is for the Ni compound at 68 K.

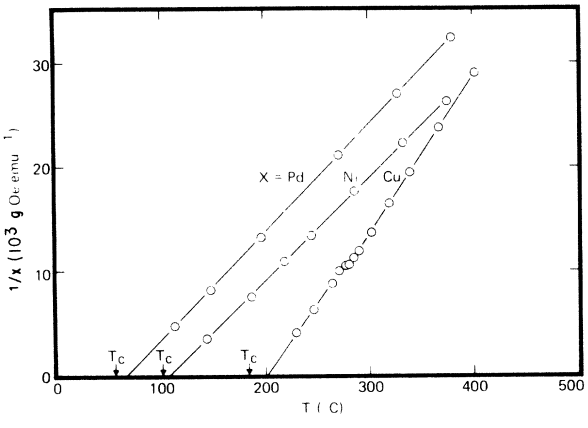

FIG. 6. Reciprocal susceptibility vs temperature for the Ni, Pd, and Cu compounds. Ferromagnetic Curie temperatures are also indicated for each compound.

relative to the metal atoms, the bonding orbitals are primarily Bi 6*s* and 6*p* bands and the nonbonding and antibonding orbitals are primarily metal-atom *s* and *p* bands. Moreover, the 24 orbitals per formula unit, though nonbonding with respect to the metal-Bi interactions, form broad metal-atom conduction bands that overlap the metal-atom *d* bands as in a transition-element metal or alloy. Since even with a formal valence 3− at the Bi atoms the average valence state at a metal atom is $<2+$, it is reasonable to anticipate that the bonding *s* and *p* bands are filled. Therefore, we make the following assumption:

Assumption 1. The bonding orbitals (primarily Bi 6*s* and 6*p* bands) are filled, from which it follows that the number n_d of *d* electrons per formula unit is

$$n_d = n - 32 - n_s \,, \tag{1}$$

where n is the total number of outer electrons and n_s the number of metal-atom *s* electrons per formula unit.

In the transition elements, $n_s < 1$ per atom. In the compound, overlap of *s* and *d* bands is reduced by the formation of antibonding orbitals. Therefore, we make the following assumption:

Assumption 2. The antibonding orbitals (primarily metal-atom *s* and *p* bands) are empty, from which it follows that the parameter n_s is constrained to the limits

$$0 < n_s < 3 \,. \tag{2}$$

The schematic density-of-states–versus–energy curves shown in Fig. 8 conform to these assumptions.

In order to distinguish the strongly correlated *d* electrons from the itinerant *d* electrons and to establish the relative stabilities of the various *d* bands, it is necessary to investigate the point symmetries at the metal-atom sites. From Fig. 7(a), an octahedral site is orthorhombic and the *d*-orbital identifications relative to the indicated local axes are the following:

$$a_{1e} = d_{z^2} \,,$$

strongly antibonding with respect to Bi at 8*c*;

$$b_{1e} \approx d_{xy} \,,$$

strongly antibonding with respect to Bi at 24*e*;

$$b_{3t} \approx d_{yz} \,,$$

moderately antibonding with respect to Bi at 8*c*;

$$a_{1t} \approx d_{x^2-y^2} \,,$$

forms narrow tetrahedral-octahedral (tet-oct) band states with Mn/*X* at 32*f*;

$$b_{2t} \approx d_{xz} \,,$$

forms broader tetrahedral-octahedral (tet-oct) band states with Mn/*X* at 32*f*.

From Fig. 7(b), a tetrahedral site has trigonal symmetry, and the *d*-orbital identifications are the following:

$$a_{1t} = d_{z'^2}$$

strongly antibonding with respect to Bi at 8*c*;

$$e_t \approx d_{y'z'} \,,\ d_{z'x'} \,,$$

form tet-oct band states with Mn at 24*d*;

$$e \approx d_{x^2-y^2} \,,\ d_{z^2} \,,$$

form tetrahedral-tetrahedral (tet-tet) band states among Mn or *X* at 32*f*.

Assertion of the formation of narrow *d* bands on the metal-atom array is based on the following assumption:

Assumption 3. Metal-metal separations < 3.0 Å at room temperature are short enough for the formation of itinerant-electron *d* bands.[2] The tet-oct site separation is only 2.8 Å and the tet-tet sepa-

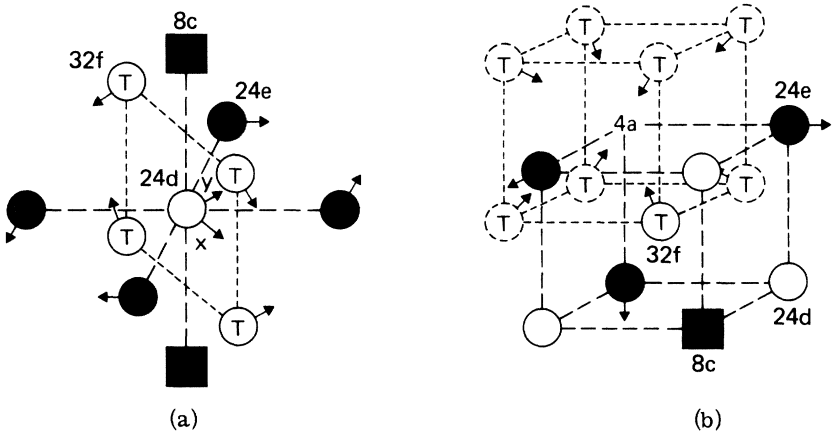

FIG. 7. Near-neighbor configuration at (a) octahedral Mn at 24d and (b) tetrahedral Mn (or *X*) at 32*f*. Diagram (b) also shows the octet of tetrahedral Mn or *X* about the empty 4*a* site.

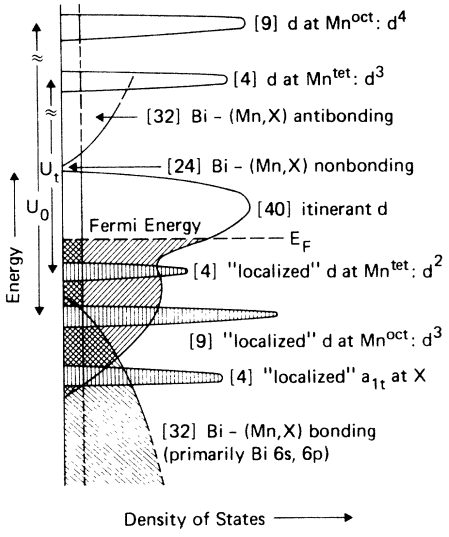

FIG. 8. Schematic density-of-states vs energy for $Mn_2X_2[Mn_3]Bi_4$. Numbers in brackets indicate number of states per molecule.

ration is 2.6 Å for X = Ni and 2.8 Å for X = Pd.

Although the d electrons are antibonding with respect to the Bi array, they may be bonding, nonbonding, or antibonding with respect to the metal-atom array. Since there are four tetrahedral-site atoms per formula unit and each contributes two e orbitals, there are eight bonding and eight antibonding states per formula unit (two spin states per orbital) in the tet-tet bands. Note that tet-tet and tet-oct bands refer to energy bands containing states formed, respectively, from the tetrahedral site e orbitals and from mixtures of tetrahedral e_t and octahedral a_{1t}, b_{2t} orbitals.

Because there are four tetrahedral-site atoms and only three octahedral-site atoms (each atom contributing two orbitals or four states to the tet-oct bands), the tet-oct bands contain 12 bonding, 12 antibonding, and four tetrahedral-site nonbonding states per formula unit. In Fig. 8, the 20 bonding (8 tet-tet + 12 tet-oct) and 20 antibonding itinerant-electron states are indicated by a bimodal density-of-states–versus–energy curve, the bottom half representing bonding states and the top half antibonding states. No attempt has been made to distinguish the relative stabilities and widths of the tet-tet and tet-oct bands. However, the fact that the d orbitals at Ni, Pd, and Cu atoms are more stable than those at Mn atoms introduces, implicitly in Fig. 8, the following assumption:

Assumption 4. In the presence of Mn atoms having more than four d electrons, Ni, Pd, and Cu atoms have filled d orbitals.

Ordering of Ni, Pd, or Cu atoms on tetrahedral sites makes it possible to assign all their e_t electrons to bonding tet-oct band states. Ordering of X atoms among the tetrahedral sites would make it possible to assign all their e electrons to bonding tet-tet band states. Therefore, for the case of ordering of X atoms among the tetrahedral sites, Fig. 8 need not be modified to account for the greater stability of the X-atom d orbitals. However, implicit to the diagram is a confinement of the d holes to the Mn-atom array.

Observation of a large ferromagnetic moment introduces the following assumptions:

Assumption 5. The Mn-Bi-Mn interactions are weak enough that the octahedral a_{1e}, b_{1e}, and b_{3t} orbitals are strongly correlated.

Assumption 6. The tetrahedral-octahedral bands are narrow enough that the four nonbonding states per formula unit are strongly correlated.

Assumption 7. The itinerant-electron bonding states are spin-paired, but the itinerant-electron antibonding states are magnetized.[3]

Assumption 8. The strongly correlated electrons at Mn atoms occupy half-filled orbitals, a d^3 manifold at octahedral sites and a d^2 manifold at tetrahedral sites, whose energies are separated from d^4 and d^3 manifolds, respectively, by intra-atomic electron-electron Coulomb energies.[2,3]

Assumption 9. The Mn-Bi-Mn interactions, which would be antiferromagnetic according to the rules for superexchange,[3] are weaker than ferromagnetic metal-metal interactions, provided each octahedral Mn atom sees at least two X-atom nearest neighbors.

Assumptions 5–9 are self-consistent. Strongly correlated d electrons are characterized by a splitting of d^n and d^{n+1} multielectron manifolds and a contribution to the spontaneous magnetic moment equivalent to that for localized electrons. Half-filled, strongly correlated orbitals at Mn atoms correspond to maximum intra-atomic-exchange stabilization and maximum splitting of d^n and d^{n+1} manifolds. Moreover, the existence of four to five outer d electrons at the Mn atoms would seem to dictate half-filled orbitals. In addition, if the antibonding bands are narrow enough to sustain spontaneous ferromagnetism (magnetic polarization of the itinerant-electron bonding and antibonding states is not shown in Fig. 8), the nonbonding d electrons must also be magnetized—and hence strongly correlated. Since the two nonbonding orbitals (four states include spin degeneracy) belong to the tetrahedral-site array and all the X-atom e orbitals are bonding, this places one of each at the tetrahedral Mn atoms. Therefore, in Fig. 8 the d^n manifolds are an octahedral-site Mn : d^3 and a tetrahedral-site Mn : d^2. The empty d^{n+1} manifolds above E_F are separated from the d^n manifolds by

TABLE II. Predicted electron distribution and molecular moments for ordered compounds.

Formula	n	n_d	Local at oct[a]	Local at tet Mn[a]	Local at tet X	tet-tet itinerant bonding	tet-tet itinerant antibonding	tet-oct itinerant bonding	tet-oct itinerant antibonding	oct μ_{Mn}/μ_B	tet μ_{Mn}/μ_B	μ/μ_B
$Cu_4[Mn_3]Bi_4$	85	$53-n_s$	9	···	12	8	8	12	$(4-n_s)$[a]	$\frac{1}{3}(13-n_s)$	···	$(13-n_s)$
$Mn_2Ni_2[Mn_3]Bi_4$	75	$43-n_s$	9	4	4	8	n_t[a]	12	$(6-n_s-n_t)$[a]	3	$(5-\frac{1}{2}n_s)$	$(19-n_s)$
$Mn_2Pd_2[Mn_3]Bi_4$	75	$43-n_s$	9	4	4	8	n_t[a]	12	$(6-n_s-n_t)$[a]	3	$(5-\frac{1}{2}n_s)$	$(19-n_s)$
$Mn_2Rh_2[Mn_3]Bi_4$	73	$41-n_s$	9	4	4	8	n_t[a]	12	$(4-n_s-n_t)$[a]	3	$(4-\frac{1}{2}n_s)$	$(17-n_s)$

[a]Contributes an equivalent number of Bohr magnetons/formula unit to Mn moments.

the Coulomb energies U_0 and U_t. The strongly correlated (localized) electrons contribute $3\mu_B$ to the moment of each octahedral Mn atom and $2\mu_B$ to the moment of each tetrahedral Mn atom.

Unlike strongly correlated electrons, which exhibit a maximum contribution to the atomic moment if half-filled, spontaneous ferromagnetism among itinerant electrons is a maximum if the bands are $\frac{1}{4}$ or $\frac{3}{4}$ filled and would vanish if they were half-filled.[2,3] (Spontaneous magnetism of half-filled orbitals is antiferromagnetic.) Although the number of d electrons at a Mn atom is less than five, the tet-tet and tet-oct bands are more than half-filled because each X atom carries ten d electrons. The number of antibonding electrons is sufficient to ensure ferromagnetic-versus-antiferromagnetic correlations among the itinerant electrons,[3] provided the d electron-poor Mn ions do not cluster. In a Mn-rich cluster, some Mn atoms would be coupled antiparallel because the antibonding-electron concentration is diminished. Figure 8 corresponds to ordering of the X atoms among tetrahedral sites.

The construction of Fig. 8 leaves, in addition to an uncertainty in the value of n_s, an uncertainty in the distribution of the Mn d electrons. On the tetrahedral sites, the bonding e electrons are spin paired at the X atoms and n_t antibonding electrons per formula unit occupy the Mn-atom e orbitals. These contribute $(n_t/2)\mu_B$ to the moment of each tetrahedral-site Mn atom. The total number of antibonding d electrons per formula unit is n_t+n_0, where n_0 are in tet-oct bands. The spin-paired X-atom e_t orbitals account for $\frac{2}{3}$ of the bonding electrons in the tet-oct bands. Four Mn-d electrons per formula unit must also occupy spin-paired, tet-oct bonding orbitals. If these were distributed equally among all the Mn atoms, there would be 0.8 bonding d electrons per Mn atom, and the sum of "localized" plus bonding d electrons per Mn atom would be 2.8 and 3.8 for tetrahedral and octahedral sites, respectively. The total number of antibonding d electrons per formula unit is

$$n_t+n_0=n_d-37=6-n_s\,, \tag{3}$$

the number 37 being composed of 13 "localized" Mn electrons, 4 X-atom a_{1t} electrons, and 20 bonding electrons. In order to equalize the total d-electron distribution among the Mn atoms, we make the following assumption:

Assumption 10. If $n_s \geq 1$, so that $\frac{1}{5}(6-n_s)<1$ antibonding electrons per Mn atom are present, all the antibonding electrons are at the tetrahedral-site Mn atoms.

The significance of this assumption is that all the moment $(6-n_s)\mu_B$ per formula unit contributed by the (n_t+n_0) antibonding electrons appears at the two tetrahedral-site Mn atoms and none at the octahedral-site Mn atoms, so that

$$\mu_{Mn}(\text{oct})=3\mu_B \text{ and } \mu_{Mn}(\text{tet})=(5-\tfrac{1}{2}n_s)\mu_B\,. \tag{4}$$

In this case, the distribution among n_t and n_0 has no consequence for the magnetic properties. Moreover, the separation between octahedral sites is relatively large, so that antiferromagnetic coupling between octahedral-site Mn atoms is dominated by the ferromagnetic coupling between tetrahedral and octahedral Mn atoms. Implicit in Eq. (4) is the following assumption:

Assumption 11. The Mn-atom moments may be described, to first order, by a spin-only spectroscopic splitting factor, $g=2$, since the orbital momentum is quenched by the crystalline fields.

Table II summarizes the above assumptions for the compounds $Mn_2X_2[Mn_3]Bi_4$, X=Ni, Pd or Rh, and for $Cu_4[Mn_3]Bi_4$. It is assumed that the d orbitals of Rh and Cu, as well as those for Ni and Pd, are completely filled in the presence of Mn atoms. The model is seen to provide a quantitative prediction of the atomic and molecular moments of the atomically ordered ferromagnetic compounds in terms of one adjustable parameter n_s, where $0<n_s<3$. The model also indicates that, in the absence of X-atom ordering among the tetrahedral sites, there may be Mn-rich clusters within which a Mn-atom moment is coupled antiparallel at low temperatures.

In order to compare the model with paramagnetic data, it is possible to calculate a Curie constant:

$$C_{\text{mol}}=\tfrac{1}{8}[3p_{\text{oct}}^2+2p_{\text{tet}}^2]\,,$$
$$p^2=(\mu_{Mn}/\mu_B)[(\mu_{Mn}/\mu_B)+2]\,, \tag{5}$$

and $p_{\text{tet}}=0$ for $Cu_4[Mn_3]Bi_4$. Both low-temperature magnetization and high-temperature paramag-

TABLE III. Experimental and predicted moment and susceptibility.

	Low temperature moment (μ_B/molecule)		Molar Curie constant	
	Experiment	Calculated[a]	Experiment	Calculated
$Mn_3Cu_4Bi_4$	11.4	11.4	8.3[b]	8.3
$Mn_5Ni_2Bi_4$	14.1	17.4	12.4	12.1
$Mn_5Pd_2Bi_4$	13.7	17.4	12.7	12.1

[a]Calculated for $n_s = 1.6$ and perfect atomic order.
[b]$T > 280\,^\circ$ C.

netic data for $Cu_4[Mn_3]Bi_4$ can be fit, (see Table III), with

$$n_s = 1.6\,, \tag{6}$$

which falls nicely within the prescribed limits for this adjustable parameter. For comparison with experiment, $n_s = 1.6$ is chosen in Table III for the $Mn_2X_2[Mn_3]Bi_4$ compounds as well. The fact that the calculated moment is larger than found experimentally implies the existence of some (up to 10% in X = Ni) antiparallel Mn-atom moments at low temperatures. As already noted, the field dependence of the magnetization at 4.2 K provides evidence for some antiparallel moments in $Mn_2Ni_2[Mn_3]Bi_4$. At highest temperatures, where all the short-range antiparallel atomic moments are decoupled, the reciprocal susceptibility versus temperature should approach a straight line that gives a Curie constant close to the theoretical value. The situation is presumably analogous to nearly ordered Ni_3Mn and to the Heusler alloy $MnCu_2Sb$, where Mn-Ni-Mn or Mn-Cu-Mn interactions are ferromagnetic and nearest-neighbor Mn-Mn interactions are antiferromagnetic.

V. CONCLUSIONS

A consistent description of the crystal structure, magnetic properties, and schematic band structure of the $Mn_5X_2Bi_4$ family of compounds has been achieved. However, quantitative comparison of the predicted and measured magnetic properties appears to be influenced by lack of ordering of the X atoms among the tetrahedral sites. The apparent success of the model supports the several assumptions on which it is based. These include general assumptions that have proven useful for the interpretation of other magnetic compounds. This exercise provides another, quite complex, illustration of how quantitative predictions about atomic moments may be obtained from general physical arguments without a detailed knowledge of the band structure.

ACKNOWLEDGMENTS

The authors wish to thank G. Guthmiller and R. E. DeBrunce for technical assistance. We are especially grateful to Dr. W. Parrish and Dr. D. Taupin for providing the experimental integrated intensity x-ray data.

*The Lincoln Laboratory portion of this work was sponsored by the U. S. Department of the Air Force.

[1]G. B. Street, J. C. Suits, and Kenneth Lee, Solid State Commun. 14, 33 (1974).
[2]J. B. Goodenough, J. Solid State Chem. 7, 428 (1973).
[3]J. B. Goodenough, *Magnetism and the Chemical Bond* (Interscience, New York, 1963).
[4]W. Parrish, *X-ray Analysis Papers* (Centrex, Eindhoven, 1965).
[5]W. Parrish, Z. Kristallogr. 127, 200 (1968), Sec. III.
[6]D. Taupin, J. Appl. Crystallogr. 6, 266 (1973).
[7]D. Taupin, J. Appl. Crystallogr. 6, 380 (1973).
[8]M. J. Buerger, *Vector Space* (Wiley, New York, 1959).
[9]M. J. Buerger, *Crystal Structure Analysis* (Wiley, New York, 1960), p. 265.
[10]D. K. Smith, Lawrence Radiation Laboratory Report No. UCRL-50264 (unpublished).
[11]L. Néel, J. Phys. Radium 9, 184 (1948); W. F. Brown, Phys. Rev. 60, 139 (1941).